Molecular Biology of the Cell
Vol. 18, 2716–2727, July 2007

Urokinase Receptor Cleavage: A Crucial Step in Fibroblast-to-Myofibroblast Differentiation

Audrey M. Bernstein,* Sally S. Twining,† Debra J. Warejcka,† Edward Tall,* and Sandra K. Masur*‡

Departments of *Ophthalmology and ‡Structural and Chemical Biology, Mount Sinai School of Medicine, New York, NY 10029; and †Department of Biochemistry, Medical College of Wisconsin, Milwaukee, WI 53226

Submitted October 12, 2006; Revised April 24, 2007; Accepted May 3, 2007
Monitoring Editor: M. Bishr Omary

Fibroblasts migrate into and repopulate connective tissue wounds. At the wound edge, fibroblasts differentiate into myofibroblasts, and they promote wound closure. Regulated fibroblast-to-myofibroblast differentiation is critical for regenerative healing. Previous studies have focused on the role in fibroblasts of urokinase plasmingen activator/urokinase plasmingen activator receptor (uPA/uPAR), an extracellular protease system that promotes matrix remodeling, growth factor activation, and cell migration. Whereas fibroblasts have substantial uPA activity and uPAR expression, we discovered that cultured myofibroblasts eventually lost cell surface uPA/uPAR. This led us to investigate the relevance of uPA/uPAR activity to myofibroblast differentiation. We found that fibroblasts expressed increased amounts of full-length cell surface uPAR (D1D2D3) compared with myofibroblasts, which had reduced expression of D1D2D3 but increased expression of the truncated form of uPAR (D2D3) on their cell surface. Retaining full-length uPAR was found to be essential for regulating myofibroblast differentiation, because 1) protease inhibitors that prevented uPAR cleavage also prevented myofibroblast differentiation, and 2) overexpression of cDNA for a noncleavable form of uPAR inhibited myofibroblast differentiation. These data support a novel hypothesis that maintaining full-length uPAR on the cell surface regulates the fibroblast to myofibroblast transition and that down-regulation of uPAR is necessary for myofibroblast differentiation.

INTRODUCTION

Myofibroblast differentiation from fibroblasts is a critical component of the healing process. Regenerative healing (without scarring) results from the successful execution of what have been characterized as three distinct phases of wound healing. In the first phase, fibroblasts that migrate into the wound secrete proteases, extracellular matrix (ECM) molecules, and growth factors. In the second phase, fibroblasts differentiate into nonmotile, wound-contracting myofibroblasts that also secrete ECM proteins and remodel the ECM (Jester *et al*., 1995; Mohan *et al*., 2003; Netto *et al*., 2005). In the third phase, after wound closure, myofibroblasts usually disappear by apoptosis (Desmouliere *et al*., 1995). Pathological states such as hypertrophic scars, liver cirrhosis, idiopathic lung fibrosis, and glomerulosclerosis are characterized by the persistence of myofibroblasts, which contribute to disease progression by overproduction of ECM and by excessive contraction (Desmouliere *et al*., 2003; Gabbiani, 2003).

To better understand the molecular basis for the fibroblast to myofibroblast transition, we have focused on the role of the urokinase plasmingen activator (uPA) pathway during wound healing. uPA is an extracellular serine protease that binds to its receptor, uPAR, and generates plasmin from plasminogen at the cell–matrix interface. Plasmin is a broad-spectrum protease that not only cleaves fibrin and other ECM proteins but also promotes cell migration by activating matrix-sequestered metalloproteinases and growth factors (Ragno, 2006). In addition to the generation of plasmin, uPA binding to uPAR stimulates the interaction of uPAR with integral membrane proteins, such as integrins, which signal intracellularly to promote cytoskeletal reorganization and cell migration (Blasi and Carmeliet, 2002). In earlier work, we discovered that fibroblast activation is characterized by induction of the uPA pathway and that uPA binding to uPAR initiates the association of uPAR with cortical actin, distributing uPA/uPAR over the entire cell surface (Bernstein *et al*., 2004). In the current study, the importance of uPA/uPAR activity and expression to myofibroblast differentiation was investigated.

uPAR has three extracellular domains, termed D1D2D3. The D1 domain is the principal uPA binding domain (Behrendt *et al*., 1991), which can be cleaved from the full-length protein by proteases such as plasmin, uPA, trypsin, chymotrypsin, elastase, cathepsin G, and metalloproteases (Montuori *et al*., 2005). Full-length uPAR binds to uPA, integrins, and the matrix molecule vitronectin, whereas cleaved uPAR (uPAR-D2D3) cannot (Behrendt *et al*., 1991; Hoyer-Hansen *et al*., 1997; Montuori *et al*., 1999). The downstream effects of uPAR cleavage are the inhibition of uPA protease activity and uPA-induced intracellular signaling; the inhibition of the interaction of uPAR with, and regulation of, integrins, which results in an integrin-dependent increase in cell adhesion on collagen, fibronectin, and laminin; and a decrease in uPA-stimulated cell migration (Montuori *et al*., 2002). Because the transition from full-length to cleaved uPAR affects uPA-stimulated signaling and the interaction of the cell with matrix, it represents an important regulatory step, mediat-

This article was published online ahead of print in *MBC in Press* (http://www.molbiolcell.org/cgi/doi/10.1091/mbc.E06–10–0912) on May 16, 2007.

Address correspondence to: Audrey M. Bernstein (audrey.bernstein@mssm.edu).

ing both cell migration and cell adhesion. Enhanced cell adhesion stimulates myofibroblast differentiation, because stabilized cell attachment to ECM generates the cell tension required for assembly of α-smooth muscle actin (SMA) into stress fibers (Hinz and Gabbiani, 2003). These stress fibers are characteristic of the myofibroblast (Tomasek *et al*., 2002).

uPA activity is also modulated through the uPA inhibitor PAI-1, which forms a complex with uPA/uPAR and integrins on the cell surface and promotes endocytosis (down-regulation) of the complex through the low-density lipoprotein receptor-related protein (Webb *et al*., 1999; Czekay *et al*., 2001, 2003). PAI-1 was initially identified as an inhibitor of uPA; however, data now show that the PAI-1–induced endocytosis of uPAR is followed by reemergence of uPAR and integrin on the cell surface This cycling is thought to promote the detachment and attachment of cells necessary for cell migration (Nykjaer *et al*., 1997; Czekay *et al*., 2003; Stefansson and Lawrence, 2003).

To study the role of uPA/uPAR in myofibroblast differentiation, primary cells from human corneal stroma were used in an in vitro wound model in which addition of fibroblast growth factor (FGF)-2 promotes the fibroblast phenotype and addition of transforming growth factor (TGF)β promotes the myofibroblast phenotype (Maltseva *et al*., 1998). Wound healing in the cornea is of particular importance, because the restoration of corneal transparency after wounding is paramount to unimpeded vision. Because of the diverse roles attributed to fibroblasts and myofibroblasts in wound healing, we predicted that the uPA/uPAR pathway would be differentially expressed in these two phenotypes. Data from the current study suggest that maintaining full-length uPAR on the cell surface regulates the transition from migrating fibroblasts to adherent myofibroblasts. A better understanding of myofibroblast differentiation will aid in the prevention of fibrotic disease.

MATERIALS AND METHODS

Antibodies and Reagents

Mouse monoclonal antibodies made to the D1 (3931) and D2 (3932) domains of uPAR, PAI-1 (379), and tissue-type plasminogen activator (tPA) (ESP-2), the two-chain recombinant tPA activity standard (179), high-molecular-weight uPA (128), human glu-plasminogen (400), and Spectrozyme PL (251L) were from American Diagnostica (Stamford, CT). Phalloidin-rhodamine and α-smooth muscle actin-cy3 mouse monoclonal antibody (mAb) were from Sigma-Aldrich (St. Louis, MO). Cathepsin G antibody was from (Chemicon International, Temecula, CA). Protease inhibitors E-64, pepstatin, aprotonin, leupeptin, 4-(2-aminoethyl)benzenesulfonyl fluoride (AEBSF), and chymostatin were from Calbiochem (San Diego, CA). GM6001 was from Chemicon International. Extracellular signal regulated kinase (ERK)1 antibody was from Transduction Laboratories (Lexington, KY). Mouse anti-immunoglobulin (Ig)G Alexa Dye-488 and mouse anti-IgG Alexa Dye 568 were from Invitrogen (Carlsbad, CA), and normal mouse serum was from Jackson ImmunoResearch Laboratories (West Grove, PA). The uPAR constructs (wild type [WT], noncleavable, and D2D3) were a generous gift of Dr. Lilliana Ossowski (Mount Sinai School of Medicine, New York, NY). The construction of these vectors was described previously (Liu *et al*., 2002). Enhanced green fluorescent protein (EGFP)-C1 was from Clontech (Mountain View, CA). Human hepatic stellate cells (LX2) were a generous gift of Dr. Scott Friedman (Mount Sinai School of Medicine, New York, NY). Normal human lung fibroblasts (LL24) were from American Type Culture Collection (Manassas, VA).

Preparation of Corneal Keratocytes, Fibroblasts, and Myofibroblasts

Keratocytes are the quiescent cells in the normal corneal stroma that, upon wounding, are activated to become fibroblasts and myofibroblasts (Weimar, 1957; Nakayasu, 1988). They have no relationship to keratinocytes of the skin, which are epithelial. Human corneas not suitable for transplantation were obtained from either the Lion's Eye Bank (Manhasset, NY) or National Disease Research Interchange (Pittsburgh, PA). Corneas dissected from the limbus were cut into small pieces and incubated overnight at 4°C with 5 mg/ml Dispase II (Roche Diagnostics, Mannheim, Germany), antibiotic-antimycotic mix (penicillin, streptomycin, and amphotericin Bl) (ABAM), and gentamicin solution, in DMEM supplied with Ham's nutrient mixture F-12 (DMEM-F12) without sodium bicarbonate (all from Sigma-Aldrich). The next day, after shaking at 37°C for 30 min, the epithelium was released from the stroma, and it was discarded. The stromal pieces were strained and subjected to two sequential collagenase incubations of 500 U/ml (Sigma-Aldrich). The supernatant of the second collagenase incubation, containing the keratocytes, was centrifuged at 3000 rpm for 5 min.

To model the wounded corneal stromal cells, we used an established in vitro cell culture system. Keratocytes (the unwounded phenotype) were freshly isolated and evaluated without culturing. To produce fibroblasts, freshly isolated corneal stromal keratocytes as prepared above were cultured in DMEM-F12 with antibiotics plus 10% fetal bovine serum (FBS; Invitrogen), because in the presence of serum, keratocytes differentiate into fibroblasts (Masur *et al*., 1993). These fibroblasts were either maintained as fibroblasts in this media or induced to become myofibroblasts as described below. At confluence, the fibroblasts were passaged by trypsinization (Invitrogen) at a 1:3 split and used for up to eight passages. The standard protocol for maintaining fibroblasts and generating myofibroblasts for use in experiments was as follows. To maintain fibroblasts, cells were trypinized, resuspended in DMEM-F12 plus trypsin inhibitor (Sigma-Aldrich) and 0.2% bovine serum albumin, and pelleted by centrifugation. The cells were resuspended in supplemented serum-free media (SSFM): DMEM-F12, 1× RPMI 1640 Vitamin Mix, 1× ITS Liquid media supplement (5 μg/ml each of insulin, transferrin, and 0.05 μg/ml sodium selenite), 1 μg/ml glutathione (all from Sigma-Aldrich), 1 mM sodium pyruvate, 0.1 mM minimal essential medium nonessential amino acids (Invitrogen) with ABAM and gentamicin (Sigma-Aldrich) (Jester *et al*., 1999) with 10 ng/ml FGF-2 (Invitrogen) and 5 μg/ml heparin (Sigma-Aldrich). This is referred to as SSFM-FGF. Cells were then plated onto collagen 10 μg/ml (Vitrogen; Cohesion, Palo Alto, CA) in this media. To promote human corneal myofibroblast differentiation, trypinized fibroblasts were resuspended and pelleted by centrifugation as described above, and then they were resuspended in SSFM with 1.0 ng/ml TGFβ1 (R&D Systems, Minneapolis, MN) (SSFM-TGFβ), plated onto collagen, and grown for 3 d with a change of medium and growth factor after 48 h, which is necessary to maintain viable cells. As demonstrated by either an absence or presence of α-SMA–containing stress fibers, this protocol produces a pure population of fibroblasts and myofibroblasts, respectively (Warejcka *et al*., 2005). In contrast, the phenotype of the cells seeded on collagen in SSFM alone has not been defined and may vary with the effects of the endogenously secreted cytokines.

Plasminogen Activator (PA) Activity Assay

Cells were plated onto collagen in 60-mm tissue culture dishes at 5.0×10^4 cells/ml in either SSFM, SSFM-FGF, or SSFM-TGFβ and grown for 8, 24, 48, or 72 h. At the specified time points, cells were washed two times with phosphate-buffered saline (PBS), and then they were lysed with 0.5 ml of 0.1 M Tris-HCl, pH 8.1, with 0.1% Triton X-100 (lysis buffer), snap-frozen in methanol and dry ice, and stored at −80°C.

uPA activity was determined using a chromogenic assay for plasminogen activation. For total PA activity (uPA and tPA), 10 μl of sample was added to 105 μl of lysis buffer and 10 μl of human plasminogen (0.2 mg/ml in PBS) in a 96-well plate. To inhibit tPA activity, 10 μl of sample was first incubated with 1 μl of the inhibitory tPA antibody (ESP-2; American Diagnostica) at 1 mg/ml) at room temperature (RT) for 20 min. After incubation, the samples were centrifuged for 3 min at 14,000 rpm at 4°C. This mixture (11 μl) was added to 104 μl of lysis buffer and 10 μl of human plasminogen in a 96-well plate. After 2-h incubation at 37°C, 15 μl of chromogenic substrate for plasmin (Spectrozyme PL) was added to each well. The chromogenic substrate was prepared by diluting 50 μmol into 27 ml of lysis buffer, and then it was neutralized to pH 7.0 with 0.6 ml of 1 N HCl. The reaction product was read on a Bio-Tek spectrophotometer (405 nm; Bio-Tek, Instruments, Winooski, VT) at 1 h, and the results were compared with a standard curve that was produced by serial dilutions of high-molecular-weight uPA and tPA.

Plasminogen Activator Zymogram

Zymography using casein-plasminogen gels allowed for the identification of uPA and tPA based on molecular weight and induced enzymatic activity. Human corneal fibroblasts were grown on collagen in 60-mm dishes at 5.0×10^4 cells/ml in SSFM, SSFM-FGF, or SSFM-TGFβ for 72 h. To assay secreted PAs, 40 μl of conditioned media was diluted with 40 μl of 2× nonreducing SDS-polyacrylamide gel electrophoresis (PAGE) sample buffer. As standards, uPA and tPA (American Diagnostica) were diluted in 0.5 M Tris-HCl, pH 6.8. The standards and conditioned media were loaded onto 10% SDS-PAGE gels containing 0.2% casein (Sigma-Aldrich) and 16 μg/ml plasminogen (American Diagnostica) (Twining *et al*., 1996). After electrophoresis, the gel was washed with 2.5% Triton X-100 for 1 h with shaking at RT to allow for activation of the enzymes and cleavage of plasminogen. The gel was then incubated in casein gel buffer (50 mM Tris, pH 8.0, 5 mM $CaCl_2$, and 0.2% Na azide) for 5 h at 37°C and stained with Coomassie blue. To maintain viable cells grown in SSFM rather than media containing serum, we have found that SSFM must be replaced every 48 h. Therefore, the 72-h point for conditioned media in this assay (Figure 2E) and below (Figure 3) is collected 24 h after

replacement of media and growth factor on cells that have been grown for 72 h.

Western Blot

PAI-1 in Conditioned Media. Cells were plated in 100 mm dishes at 5.0×10^5 cells/ml on collagen in SSFM, SSFM-FGF-2, or SSFM-TGFβ1. At 72 h, 10 ml of conditioned media were removed and immediately stored on ice. From the conditioned media, 200 μl was removed and added to 40 μl of 4× SDS sample buffer with βME. From the 240 μl, 40 μl was separated on a 10% SDS-PAGE gel, transferred to nitrocellulose and processed for western blots using a PAI-1 mouse mAb (American Diagnostica). For the conditioned media at time points 8, 24, 48, and 72 h, the samples were processed as above.

PAI-1 and Cathepsin G in Cell Lysates. Cells were plated as described above in SSFM-TGFβ. At 8, 24, 48, and 72 h, cells were washed with PBS, and then they were incubated with detachment buffer (20 mM Tris, pH 7.5, 250 mM sucrose, and 1 mM EDTA) containing protease inhibitor tablet (Roche Diagnostics), and phenylmethylsulfonyl fluoride (Sigma-Aldrich) for 20 min on ice followed by scraping. Cells were pelleted at 3000 rpm and lysed with Triton buffer (1.0% Triton X-100, 140 mM NaCl, and 10 mM Tris, pH 7.4), with protease inhibitor tablet and phenylmethylsulfonyl fluoride. Lysates were thawed and centrifuged at 15,000 rpm to pellet insoluble material. Then, 20 μg of protein was separated on a 10% SDS-PAGE reducing gel, transferred to nitrocellulose, and processed for Western blots. The membranes were blocked with 5% milk in Tris-buffered saline (TBS). PAI-1 antibody was diluted to 5 μg/ml in TBS plus 1% milk followed by washing with TBS and incubation with horseradish peroxidase (HRP)-conjugated secondary antibody. The bands were visualized with chemiluminescent substrate (Pierce Chemical, Rockford, IL). After the blot was developed for PAI-1, it was reprobed without stripping for ERK1. ERK1 antibody was diluted to 1 μg/ml and processed as described above. The blots were scanned using a Kodak Image Station 440 CF, and the ratio of PAI-1 to the normalizing protein ERK1 was graphed.

For detection of cathepsin G (Figure 5C), cells were seeded on collagen and grown for 24 h in either SSFM-FGF-2 or SSFM-TGFβ. Cells were processed as described above, and the Western blot was probed with cathepsin G antibody at 1 μg/ml.

uPAR in Cell Lysates. Cells were seeded onto collagen in SSFM alone, SSFM-FGF, or SSFM-TGFβ, and media were replaced every 48 h. After a total of 72 h (Figure 4) or at time points (days 1, 2, 3, 5, and 7) (Figure 5), cells were detached, pelleted, and lysed as described above for PAI-1. Lysates were snap-frozen in dry ice and ethanol, and they were stored at −80°C. Lysates were thawed and centrifuged at 15,000 rpm to pellet insoluble material. Twenty micrograms of Triton X-100 soluble protein was separated on a nonreducing 10% SDS-PAGE gel and transferred to polyvinylidene difluoride for 2 h at 50 V. After blocking with 5% milk in Tris-buffered saline (TBS), uPAR antibody to domain D2 (American Diagnostica) was diluted to 2 μg/ml in TBS plus 1% milk followed by washing with TBS and incubation with HRP-conjugated secondary antibody and visualized as described above.

Protease Inhibitor Studies

Cells were seeded onto collagen in SSFM-TGFβ to which we added protease inhibitors chosen to determine which class of protease was cleaving uPAR. These included 10 μM E-64, 1 μM pepstatin A, 10 μg/ml aprotinin, 10 μM leupeptin, 0.5 mg/ml AEBSF, 25 μM GM6001, or 20 μM chymostatin. Concentrations were chosen according to the manufacturer's recommendations (Calbiochem). After 24 h, cells were detached, processed, and evaluated for the presence of cleaved and full-length uPAR in Western blots as described above.

Immunocytochemistry

Detecting α-SMA. Cells were grown on coverlslips coated with collagen and standardly fixed with 3% *p*-formaldehyde (Fisher Scientific, Fair Lawn, NJ) in PBS, pH 7.4 for 15 min at RT, and then they were permeabilized with 0.1% Triton X-100. (For Figure 1, the cells were placed on ice for 5 min before fixation and not treated with detergent. This facilitated antibody access to α-SMA while maintaining immunodetectable uPAR, which would be lost with Triton X-100.) After blocking nonspecific binding with 3% normal mouse serum (Jackson ImmunoResearch, West Grove, PA), the cells were incubated with antibody to α-SMA conjugated to cy3, washed in PBS, and then coverslips were mounted in Vectashield mounting medium (Vector Laboratories, Burlingame, CA) on slides for viewing with a Zeiss Axioskop microscope (Carl Zeiss, Jena, Germany). Images were captured using a Zeiss Axioscope with a SPOT-2 charge-coupled device (CCD) camera (Diagnostic Instruments, Sterling Heights, MI) and processed by Adobe PhotoShop software (Adobe Systems, Mountain View, CA).

Quantification of Full-Length and Cleaved uPAR. Cells were plated on collagen in SSFM-FGF or SSFM-TGFβ, and they were grown for 3 d. To expose surface uPAR for immunodetection, we used our previously published protocol in which the cells were "stripped" of cell surface uPA before fixation (Bernstein *et al*., 2004). Stripping was achieved by an acid wash with 0.05 M glycine and 0.1 M NaCl, pH 3.0, 1 min at RT, followed by three washes with PBS, pH 7.0 (Stoppelli *et al*., 1986; Baker *et al*., 1992). Cells were then fixed with 3% *p*-formaldehyde in PBS. To detect both full-length and cleaved uPAR, we used antibody to the D2 domain, because D2 is present in both. To detect only full-length uPAR, we used antibody that only recognizes D1. The sequence was to detect D1 first, followed by D2 detection. Specifically, after blocking nonspecific binding with 3% normal goat serum, cells were incubated with mouse anti-D1 domain uPAR antibody, at 10 μg/ml for 1 h at RT followed by washing in PBS and incubation with goat anti-mouse IgG Alexa Dye 488 for 1 h at RT. Cells were again washed with PBS, blocked with 3% mouse serum to saturate any remaining free anti-mouse IgG before the second immunodetection protocol. Cells were incubated for 1 h at RT with an anti-D2 uPAR antibody at 10 μg/ml, followed by PBS washing and incubation with a goat anti-mouse IgG Alexa Dye 568. Coverslips were mounted on slides for viewing with a Zeiss Axiovert. Axiovert images were captured with an Axiocam MRm CCD camera. To saturate cell-surface uPAR, the primary antibodies were used at a relatively high concentration chosen after preliminary studies (10 μg/ml). To control for a potential difference in the fluorescent tags linked to the secondary antibodies, the experiment was repeated, interchanging the secondaries.

We defined the image detected by anti-D2 as "total uPAR", because D2 is present is both full-length (D1D2D3) uPAR and in cleaved uPAR (D2D3), whereas we defined the image detected by anti-D1 antibody as "full-length uPAR", because D1 is present only in full-length uPAR. To quantify the relative amount of full-length uPAR to total uPAR, we captured colocalized images from the D1 domain immunostaining and D2 domain immunostaining by using identical parameters. These images were then exported into the MetaMorph image analysis software package, version 6.3r3 (Molecular Devices, Sunnyvale, CA). Threshold values were chosen to include the cells in the field and to exclude nonspecific background. Applying these parameters to the colocalized images, the pixel intensity was assessed. The ratio of full-length uPAR to total uPAR was determined by dividing the intensity of the D1 antibody immunostaining by the intensity of the D2 antibody immunostaining. The average of the ratios obtained from the FGF-2–treated cells in each experiment was considered 100%. Correspondingly, the average of the ratios obtained from the TGFβ1-treated cells was expressed as a percentage of the FGF-2–treated cells.

Transfection of uPAR Constructs. We tested the impact of overexpressing full-length, noncleavable uPAR on myofibroblast differentiation. The noncleavable uPAR cDNA as well as controls, WT-uPAR, and truncated uPAR (uPAR-D2D3) were described previously, and they were a generous gift from Dr. Lillian Ossowski (Mount Sinai School of Medicine) (Liu *et al*., 2002). All cDNAs were subcloned into a pCDFA2.1-Hyg vector (Invitrogen). The noncleavable form of uPAR contains full-length uPAR with four mutations in the protease sensitive linker between D1 and D2 of uPAR, R83K, Y87C, R89K, and R91K, which made it uncleavable. The D2D3 mutant was created by removing the sequence for the D1 domain and joining the signal sequence to the D2D3 domains. The transfection control was EGFP-C1 (Clonetech). These constructs were transfected into human corneal stromal fibroblasts using the Nucleofection system (Amaxa, Gaithersburg, MD).

Briefly, corneal stromal fibroblasts were trypsinized and resuspended in DMEM-F12 with 10% FBS without antibiotics and aliquoted into 15 ml conical tubes with 5×10^5 cells/tube. Cells were pelleted by centifugation at 3000 rpm at 4°C. The cell pellet was resuspended in 100 μl of Nucleofection reagent. To the resuspended cells, 2 μg of WT-uPAR, D2D3-uPAR, or noncleavable-uPAR plasmid and 1 μg of EGFP plasmid were added. In the control, 1 μg of only the EGFP plasmid was added. The plasmid mixture was nucleofected (electroporated) into the cells on Amaxa program U20. Cells were plated at intermediate density (5×10^3 cells/ml) onto coverslips coated with collagen in DMEM-F12 containing 10% FBS, without antibiotics. We found that plating into serum-containing media was necessary for cell viability after electroporation. After 4 h, the media were changed to SSFM with antibiotics and 1 μg/ml TGFβ1. Cells were grown for 72 h, with the media and the growth factor renewed at 48 h. The cells were then fixed, permeabilized, and immunostained with α-SMA-cy3 antibody. Cells were visualized with a Zeiss Axiovert. Axiovert images were captured with an Axiocam MRm CCD camera. The transfection efficiency was ~50% based on the presence of EGFP.

RESULTS

uPA and uPAR Are Absent from the Myofibroblast Cell Surface after 7 d

In preliminary experiments, human corneal fibroblasts were grown in media containing both serum and TGFβ1 producing a mixed culture of fibroblasts and myofibroblasts. Under these conditions, cells in contact with the coverslip were

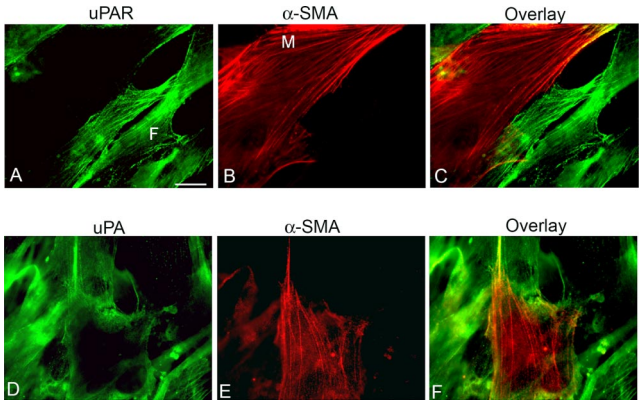

Figure 1. uPA and uPAR are absent from the myofibroblast cell surface after 7 d. Fibroblasts were seeded in serum and grown for 7 d with 1 ng/ml TGFβ1. Cells were immunostained with antibody to uPAR (made to the D2 domain (total uPAR)) (A), α-SMA (B), overlay (C), uPA (D), α-SMA (D), and overlay (F). Myofibroblasts (M) were detected by their expression of α-SMA in fibrils. uPAR was immunodetected on fibroblasts (F), but it was absent from myofibroblasts. The cells were put on ice for 5 min before fixation. This protocol allows anti-α-SMA antibodies to penetrate the membrane without the use of detergent, which would remove uPAR from the cell membrane. Bar, 20 μm. The image shown is representative of three independent experiments.

fibroblasts (F), whereas cells "sitting on top" of a confluent layer of fibroblasts were myofibroblasts (M) (Figure 1). After 7 d in this culture system, uPAR and uPA were highly expressed on the fibroblasts, whereas they were almost completely absent from the myofibroblasts (Figure 1, A and D). By placing the coverslips on ice during immunostaining, uPA/uPAR was visualized as a fibrillar pattern (A and D), presumably reflecting the interaction of uPAR with integrins, which align along cortical actin microfilaments. Most importantly, however, the observation that fibroblasts strongly expressed uPA/uPAR, whereas myofibroblasts had almost no detectable uPA/uPAR cell surface expression after 7 d, prompted us to study the regulation of uPA/uPAR during the fibroblasts transition to myofibroblasts by using culture conditions that could generate phenotypically pure cultures. To achieve pure myofibroblast cultures, fibroblasts were plated on collagen and cultured in SSFM with TGFβ. Pure fibroblast cultures were produced when cells were plated on collagen and cultured in SSFM with FGF.

PA Activity Was Increased after Treatment with FGF-2

To evaluate uPA/uPAR pathway regulation during the fibroblast-to-myofibroblast transition, we assayed for total cell-associated PA activity, in the two phenotypic culture conditions. Time points between 8 and 72 h after incubation with either FGF or TGFβ were assayed and compared with cells incubated in SSFM alone. We found that addition of FGF increased cell-associated PA activity, whereas addition of TGFβ inhibited PA activity (Figure 2A). To dissect the contributions of uPA and tPA in total PA activity, the same samples were first incubated with an inhibitory tPA antibody. This antibody inhibits tPA activity by an average of 90% ($\pm$6%), but it inhibits uPA activity by an average of only 12% ($\pm$5%) at the same concentration (Figure 2, C and D). Using this inhibitory antibody, we found that uPA constituted 40% ($\pm$9%) of the FGF-induced PA activity, whereas, uPA was only 29% ($\pm$10%) and 22% ($\pm$11%) in the TGFβ- and SSFM-induced activities, respectively. This suggested that not only does FGF-2 increase PA activity overall but also that more of the FGF-2–induced PA activity was uPA than tPA compared with TGFβ-treated cells and SSFM alone. Because we could not detect PA activity in conditioned medium using the PA assay, the more sensitive casein-plasminogen zymography was used to visualize uPA and tPA activities in cells and conditioned medium (Figure 2E). The zymogram of the cell lysates was consistent with the PA assay and correspondingly, in conditioned media uPA and tPA activity and expression were increased by FGF-2 and decreased by TGFβ1.

PAI-1 Is Secreted in Response to TGFβ1

Along with the decrease in PA expression (Figure 2E), the decrease in PA activity observed in corneal fibroblasts cultured in the presence of TGFβ (Figure 2A) could be due to increased expression and secretion of the PA inhibitor PAI-1. Confirming previous reports, we found that PAI-1 was secreted in response to TGFβ1 treatment (Figure 3A) (Abe *et al*., 1994). To evaluate the cell-associated PAI-1 throughout the period in which we measured cell-associated PA activity, PAI-1 was immunodetected in Western blots of extracts of TGFβ1-treated cells at each time point starting at 8 h (Figure 3B). Expression of PAI-1 throughout the time course may contribute to a TGFβ1-induced decrease in cell-associated PA activity (Figure 2).

uPAR Is Differentially Expressed in Keratocytes, Fibroblasts, and Myofibroblasts

Because uPAR is highly glycosylated, uPAR is visualized as a nondiscrete band(s) between the molecular weights of 35 and 50 kDa in Western blots (Figure 4A, arrows). No uPAR was detected in the resident corneal stromal cells, keratocytes, lysed immediately after isolation (not grown in culture) (Figure 4A, lane 1). The absence of immunodetected keratocyte uPAR confirms the in situ observation that uPAR is not expressed in the normal, unwounded corneal stroma (Tripathi *et al*., 1990). Full-length uPAR (D1D2D3) (Hoyer-Hansen *et al*., 1992) was detected in fibroblasts grown in SSFM-FGF 72 h (Figure 4A, lane 2). The cleaved form of uPAR (D2D3-uPAR), which lacks the D1 domain (Hoyer-Hansen *et al*., 1992), was detected as a significant component in the myofibroblast lysate, in addition to full-length uPAR (cells grown in SSFM-TGFβ 72 h; Figure 4A, lane 3). Additional experiments using corneal fibroblast cultures derived from different donors showed the same pattern but with variation in the amounts of full-length and cleaved uPAR in the FGF and TGFβ lysates (lanes 4 and 5). In every case, the proportion of full-length uPAR to cleaved uPAR was significantly greater in the FGF-treated cells than in the TGFβ-treated cells (see below).

Visualization of Full-Length and Cleaved uPAR

The biochemical data demonstrating that D2D3-uPAR was increased in myofibroblasts (Figure 4A) prompted further investigation into the proportion of cleaved-to-full-length uPAR on the cell surface of fibroblasts and myofibroblasts. Immunocytochemistry using specific antibodies generated to the D1 or D2 domain of uPAR was used to quantify and compare the relative amounts of full-length and cleaved uPAR on corneal fibroblasts and myofibroblasts. The D1 domain antibody detects only the full-length uPAR, whereas the D2 domain antibody detects total uPAR (both full-length and cleaved). Only cell surface uPAR was detected, because the cells were not permeabilized during immunocytochemical preparation. The images were captured using identical parameters, and they were not digitally altered or enhanced.

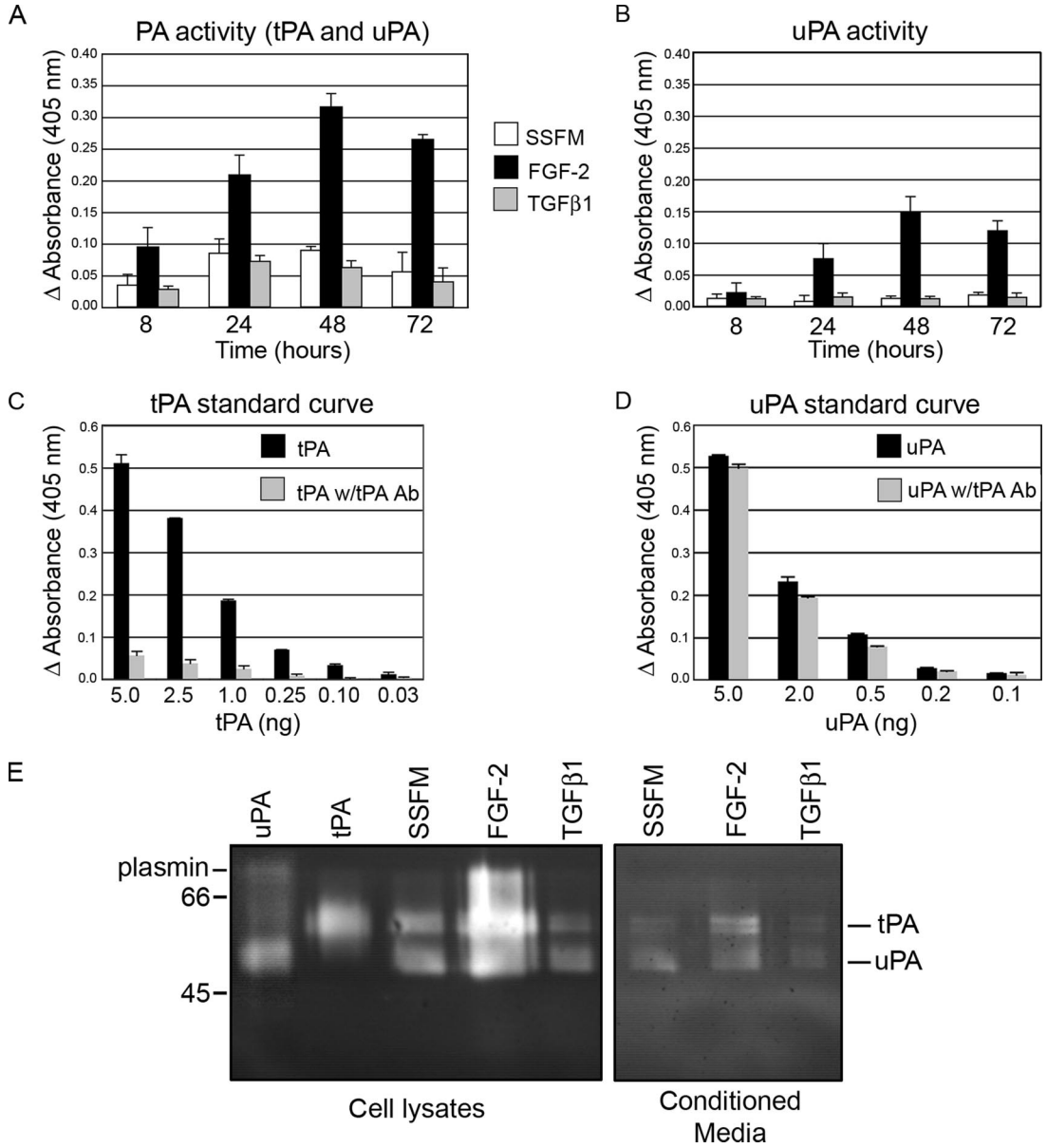

Figure 2. PA activity and expression are increased with FGF-2 and decreased with TGFβ treatment. Cellular PA activity was increased with FGF-2 treatment and inhibited by TGFβ1. (A) Cells were plated in SSFM, SSFM-FGF, or SSFM-TGFβ, and they were grown for 8, 24, 48, or 72 h. At the specified time points, cells were washed two times with PBS, and then they were lysed with 0.5 ml of 0.1 M Tris-HCl, pH 8.1 with 0.1% Triton X-100. PA activity was determined with a chromogenic assay that detected the generation of plasmin. (B) The same samples were incubated with an inhibitory tPA antibody to determine the proportion of PA activity that was uPA and tPA. (C) tPA standard curve without and with inhibitory tPA antibody. (D) uPA standard curve without and with inhibitory tPA antibody. (E) Fibroblasts were plated in SSFM, SSFM-FGF, or SSFM-TGFβ. After 72 h, lysates and conditioned media were tested for PA activity. uPA and tPA in lysates and conditioned media were increased in FGF-2–treated cells, whereas less uPA and tPA was detected in TGFβ1 treated cells. The PA assay was performed in duplicate with cells from three different donors. The zymogram is representative of three experiments with the same cells as in the PA assay (A and B).

We confirmed that without addition of exogenous uPA to initiate the association of uPAR with the actin cytoskeleton, uPA/uPAR is seen as aggregates. This is the result of a postfixation effect of primary and secondary antibody "capping" of the GPI-linked uPAR in lipid rafts when fixation was followed by immunodetection for either uPA or uPAR (Bernstein *et al*., 2004). Furthermore, comparing FGF- and TGFβ-treated cells, the full-length uPAR detected by antibody to the D1 domain demonstrated that the intensity of immunostaining was consistently and dramatically increased on FGF-treated fibroblasts, suggesting that the cleavage of full-length uPAR is either inhibited in fibroblasts and/or that full-length uPAR on fibroblasts is resynthesized over time, whereas on myofibroblasts it is not (Figure 4B). Using MetaMorph software, we analyzed the intensity of the colocalized immunostaining using cells from two different donors and found a consistent 58% ($\pm$5%) decrease in the ratio of full-length uPAR to total uPAR in myofibroblasts compared with fibroblasts (Figure 4C). To determine whether uPAR cleavage was sufficient to promote myofibro-

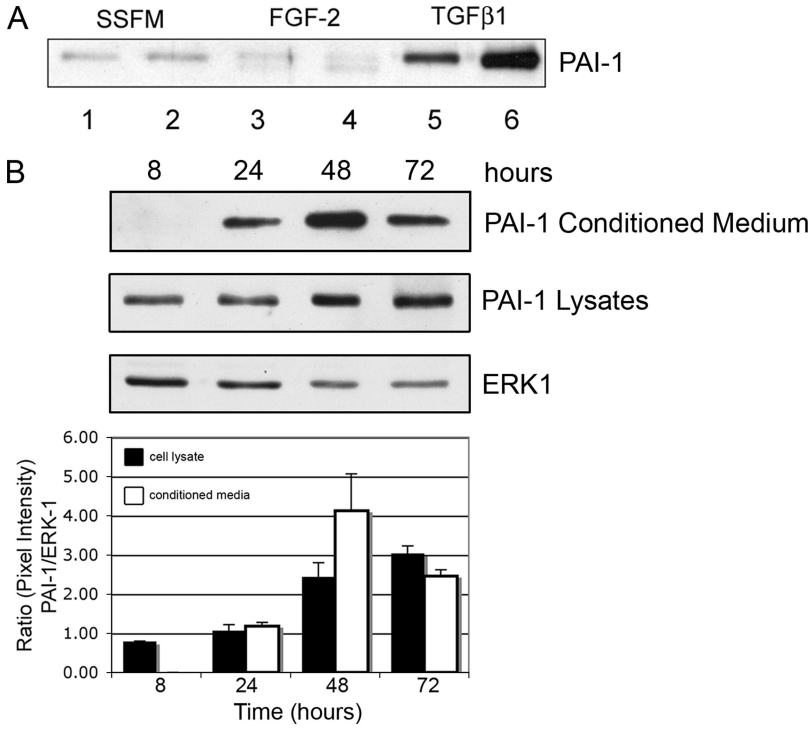

Figure 3. PAI-1 is secreted in response to TGFβ1. (A) Western blot for PAI-1. Fibroblasts were plated in SSFM, SSFM-FGF, or SSFM-TGFβ. At 72 h, conditioned media were collected and subjected to Western blot detection for PAI-1. Duplicates represent media from cells cultured from two different cornea donors. PAI-1 is labeled. TGFβ1 induced PAI-1 secretion, whereas FGF-2 did not. (B) Cells were plated in SSFM-TGFβ and grown for 8, 24, 48, or 72 h. At the specified time points, cells were lysed. Both conditioned media and lysates were detected for PAI-1 secretion and expression by Western blot. In the cells treated with TGFβ1, PAI-1 was detected in cell lysates at 8 h and in conditioned media at 24 h; expression increased with time. ERK1 expression functions as a control for protein loading. The ratio of the pixel densities (PAI-1/ERK1) is calculated and graphed. The Western blot image is representative of three independent experiments.

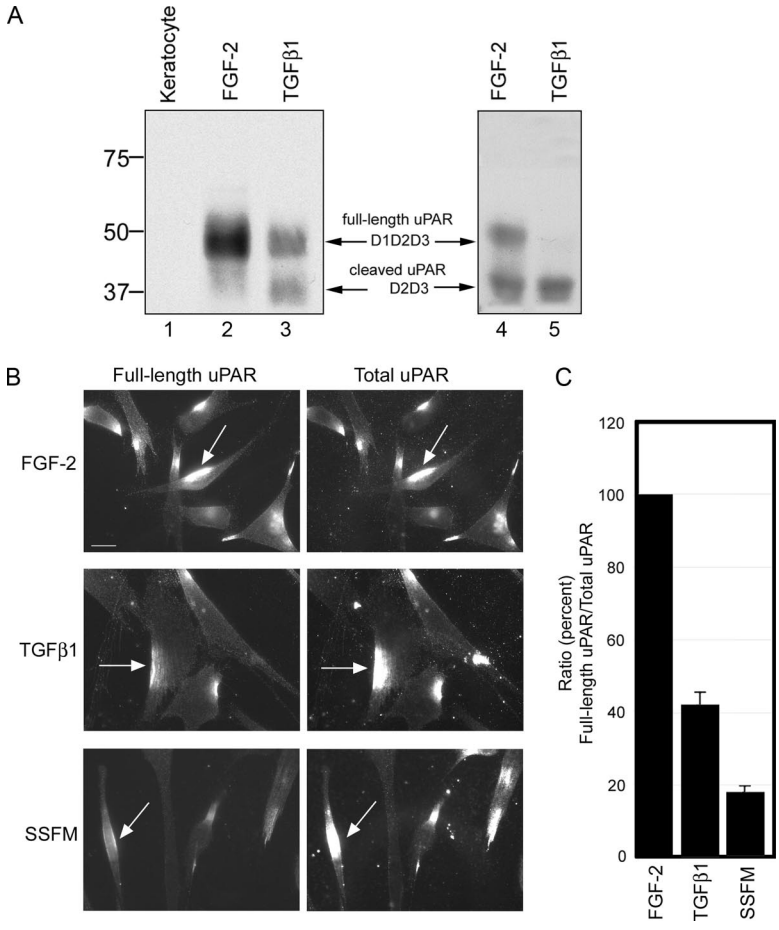

Figure 4. FGF-2–treated fibroblasts expressed more full-length uPAR than TGFβ-treated fibroblasts. By immunoblot detection and immunofluorescence, we found that cells grown for 72 h with FGF retained significantly more full-length uPAR compared with TGFβ-treated cells. Keratocytes (quiescent fibroblasts) did not express uPAR (n = 5; results from 5 different cornea donors). (A) Cell lysates were detected for the presence of total uPAR by Western blot (n = 10; results from 5 different cornea donors). Freshly isolated keratocytes (lane 1), fibroblasts plated in the presence of FGF (lanes 2 and 4), or TGFβ (lanes 3 and 5). (B) Cells were seeded in SSFM-FGF, SSFM-TGFβ, or SSFM alone, and they were grown for 72 h. To remove any uPA-bound uPAR that could block uPAR antibody binding, cells were stripped of cell surface uPA with 0.05 M glycine and 0.1 M NaCl, pH 3.0, before fixation, followed by washing with PBS (Stoppelli *et al*., 1986; Baker *et al*., 1992; Bernstein *et al*., 2004). To detect full-length uPAR, an antibody to the D1 domain of uPAR was used (see *Materials and Methods*). Total uPAR was detected with an antibody to the D2 domain, which is present in both full-length and cleaved uPAR (see *Materials and Methods*). Bar, 20 μm. (C) To quantify the relative amounts of full-length uPAR to total uPAR, colocalized images were captured with identical parameters and analyzed for their intensity using MetaMorph image analysis software. For each condition, ~20 fields from two different cornea donors were imaged and analyzed.

blast differentiation, cells treated with SSFM alone were included in the study. uPAR cleavage in SSFM-treated cells was enhanced compared with TGFβ-treated cells (82 ± 3%), suggesting that exogenously added FGF-2 and TGFβ confer regulation of uPAR cleavage that is not present in SSFM alone. However, because the concentrations of endogenous growth factors secreted from the SSFM treated cells is unknown, it is difficult to make conclusions other than uPAR cleavage in the absence of TGFβ was not sufficient to promote myofibroblast differentiation. These studies have demonstrated that myofibroblasts have more cleaved uPAR and less full-length uPAR on their cell surface after 72 h in the presence of TGFβ1 and that FGF-2 induces signals that promote the retention of full-length uPAR on the surface of the cell.

Chymostatin, AEBSF, and Serum Inhibit uPAR Cleavage and TGFβ-induced α-SMA Stress Fiber Organization

To better investigate the time frame of uPAR cleavage in cells treated with TGFβ, a time course of uPAR expression was performed. Cells were lysed at time points from 1 to 7 d and probed for total uPAR by using the D2 antibody (Figure 5A). These data show that by 24 h, cleaved uPAR was present along with some full-length uPAR. As the exposure time to TGFβ increased, full-length uPAR disappeared, and by 7 d, uPAR expression was abolished as had been visualized by microscopy in Figure 1.

To investigate which protease(s) was cleaving uPAR, cells were grown in TGFβ1 for 24 h with a panel of protease inhibitors. uPAR cleavage was not inhibited by the addition of the cysteine protease inhibitor E-64, nor the aspartate protease inhibitor pepstatin, nor the arginine/lysine protease inhibitor leupeptin, nor the matrix metalloproteinase inhibitor GM6001, but it was inhibited by the general small serine protease inhibitor AEBSF and the chymotrypsin inhibitor chymostatin (Figure 5B, lanes 1, 2, 4, 6 vs. lanes 5 and 7). We also noted that 10% FBS inhibited uPAR cleavage, although the factor present in serum that inhibits cleavage is unknown (lane 9). That AEBSF and chymostatin inhibited uPAR cleavage suggested that the protease responsible for the cleavage was a serine-type chymotrypsin-like enzyme. Because aprotinin (a general serine protease inhibitor) is ineffective against membrane-bound serine proteases such as cathepsin G, finding that aprotinin did not inhibit uPAR cleavage may suggest that the protease in question is membrane bound (Figure 5B, lane 3) (Owen and Campbell, 1998). Although originally identified in neu-

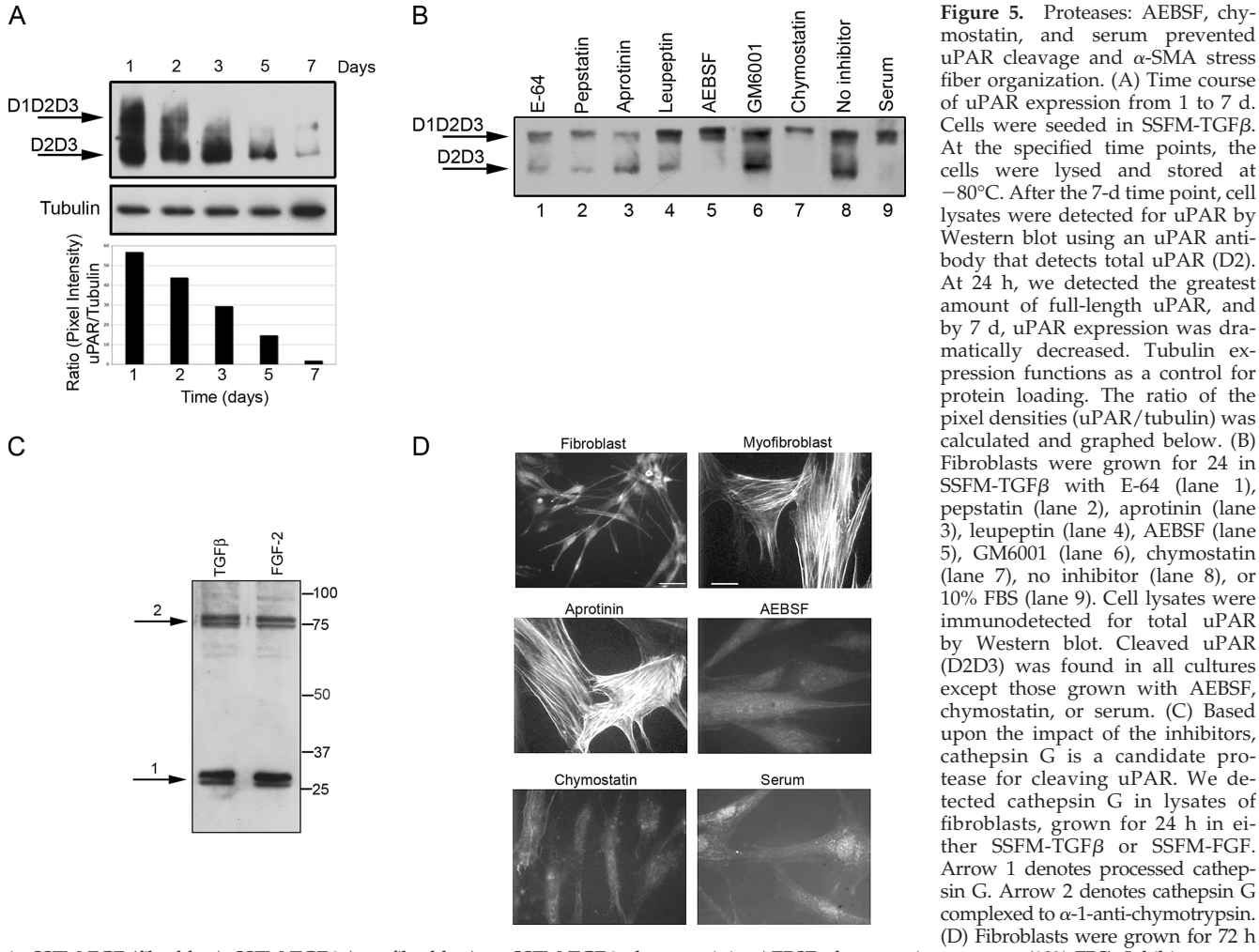

Figure 5. Proteases: AEBSF, chymostatin, and serum prevented uPAR cleavage and α-SMA stress fiber organization. (A) Time course of uPAR expression from 1 to 7 d. Cells were seeded in SSFM-TGFβ. At the specified time points, the cells were lysed and stored at −80°C. After the 7-d time point, cell lysates were detected for uPAR by Western blot using an uPAR antibody that detects total uPAR (D2). At 24 h, we detected the greatest amount of full-length uPAR, and by 7 d, uPAR expression was dramatically decreased. Tubulin expression functions as a control for protein loading. The ratio of the pixel densities (uPAR/tubulin) was calculated and graphed below. (B) Fibroblasts were grown for 24 in SSFM-TGFβ with E-64 (lane 1), pepstatin (lane 2), aprotinin (lane 3), leupeptin (lane 4), AEBSF (lane 5), GM6001 (lane 6), chymostatin (lane 7), no inhibitor (lane 8), or 10% FBS (lane 9). Cell lysates were immunodetected for total uPAR by Western blot. Cleaved uPAR (D2D3) was found in all cultures except those grown with AEBSF, chymostatin, or serum. (C) Based upon the impact of the inhibitors, cathepsin G is a candidate protease for cleaving uPAR. We detected cathepsin G in lysates of fibroblasts, grown for 24 h in either SSFM-TGFβ or SSFM-FGF. Arrow 1 denotes processed cathepsin G. Arrow 2 denotes cathepsin G complexed to α-1-anti-chymotrypsin. (D) Fibroblasts were grown for 72 h in SSFM-FGF (fibroblast), SSFM-TGFβ (myofibroblast), or SSFM-TGFβ plus aprotinin, AEBSF, chymostatin, or serum (10% FBS). Inhibitors were replaced every 24 h. α-SMA was detected by immunocytochemistry. Only the myofibroblast control and the aprotinin treated cell cultures incorporated α-SMA into stress fibers. Fibroblasts only (bar, 40 μm), myofibroblasts and inhibitor (bar, 20 μm). The images shown are representative of three experiments using two different tissue donors.

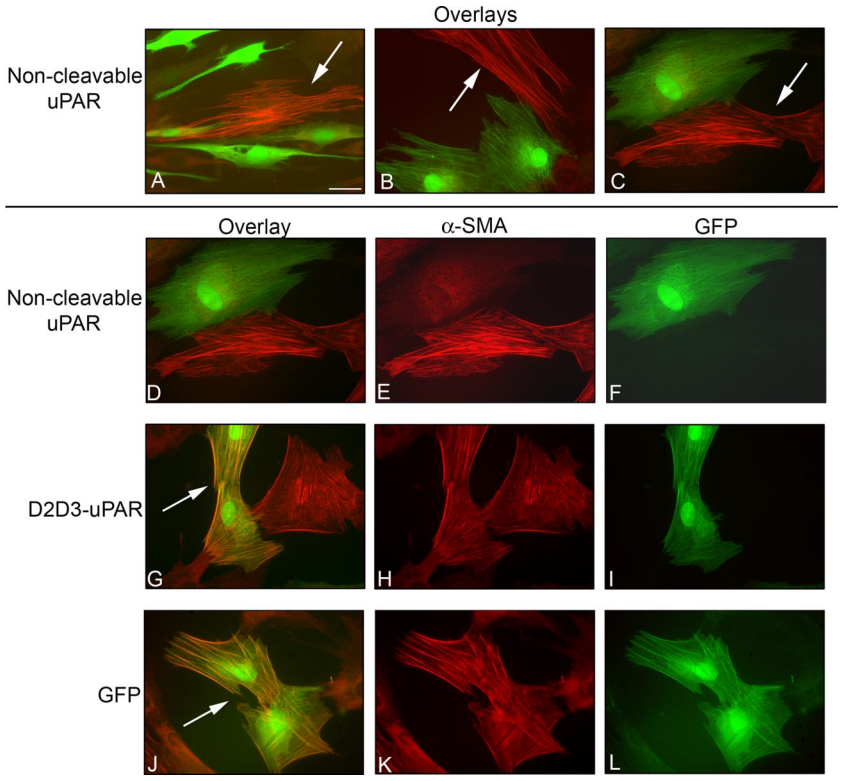

Figure 6. Noncleavable mutant uPAR inhibits myofibroblast formation. Fibroblasts were co-transfected with cDNA of noncleavable uPAR and GFP, truncated D2D3-uPAR, and GFP or GFP alone. Transfected cells were seeded in media containing 10% serum. After 4 h, media were switched to SSFM-TGFβ, and cells were grown for 72 h. Cells were immunostained for α-SMA (red), and GFP was visualized (green). The noncleavable uPAR mutant DNA inhibited myofibroblast differentiation (A–C, D–F). A–C shows colocalization overlays of three separate fields demonstrating that the cells transfected with noncleavable uPAR and GFP did not express α-SMA; therefore, they were not myofibroblasts. Cells that were not transfected with noncleavable uPAR and GFP are myofibroblasts (arrows). (D) The same field shown in (C). Each image is shown separately for α-SMA (E) and GFP (F). (G–I) Cells transfected with D2D3-uPAR and GFP. Overlay colocalization of α-SMA and GFP shows that the cells transfected with the cleaved uPAR were able to differentiate into myofibroblasts (G, arrow), α-SMA (H), and GFP (I). (J–L) GFP transfection. (J) Overlay colocalization of α-SMA and GFP shows that GFP alone did not prevent myofibroblast differentiation (J, arrow), α-SMA (K), and GFP (L). Bar, 20 μm. The images shown are representative of three experiments using two different tissue donors.

trophils, a previous study found that cathepsin G was also expressed in corneal fibroblasts (Whitelock *et al*., 1997). To confirm and extend this finding, we used commercially available antibodies to evaluate the lysates from TGFβ1 and FGF-2 treated cells for cathepsin G. Doublets at 27/29 kDa (1) and 75/77 kDa (2) were immunodetected by anti-cathepsin G in Western blots of both FGF- and TGFβ1-treated corneal fibroblasts. Doublet 1 corresponds to proteolytically processed cathepsin G (Garwicz *et al*., 1995) and doublet 2 is the correct size for cathepsin G complexed to a 50-kDa form of its endogenous inhibitor α1-antichymotrypsin, which is synthesized by corneal stromal cells (Twining *et al*., 1994). This complex can form after lysis in the lysate, and it does not dissociate under reducing conditions during electrophoresis, because they are covalently linked (Kanemaru *et al*., 1996). The expression of cathepsin G in both FGF-2– and TGFβ1-treated cells suggests that it may be active under both conditions. However, because the protease and inhibitor may form a complex in the lysate, the cellular localization of the enzyme and inhibitor cannot be inferred.

Next, we asked whether the protease inhibitors that prevented uPAR cleavage would inhibit myofibroblast differentiation. We plated cells onto collagen in the presence of TGFβ to generate myofibroblasts as indicated by α-SMA incorporation into stress fibers. Myofibroblast differentiation was prevented by inhibitors that prevented uPAR cleavage: AEBSF, chymostatin, and serum (Figure 5D). As predicted, aprotinin, which did not inhibit uPAR cleavage, also did not interfere with α-SMA stress fiber organization. Thus, inhibiting uPAR cleavage correlated with preventing myofibroblast differentiation. These data suggested that in conjunction with signals from TGFβ, sustained uPAR cleavage may be necessary to promote myofibroblast differentiation.

Noncleavable uPAR Inhibited Myofibroblast Differentiation

To further investigate the importance of retaining full-length uPAR, fibroblasts were transfected with cDNA from a noncleavable uPAR (D1D2D3) construct concurrently with a green fluorescent protein (GFP) reporter plasmid and grown with TGFβ. After 3 d, cells were fixed and immunostained for α-SMA. All transfected cells that expressed GFP, and therefore, noncleavable uPAR, resisted differentiation into myofibroblasts (Figure 6, A–C; gallery of colocalized αSMA and GFP in 3 fields), and in D–F (image C; separated into α-SMA and GFP detection). As a transfection control, we transfected other fibroblasts with a construct containing only the D2D3 domain of uPAR (uPAR-D2D3), and we asked whether myofibroblast differentiation would be induced. As expected, the cells transfected with the D2D3 mutant became myofibroblasts when grown with TGFβ unlike the cells transfected with the noncleavable D1D2D3 uPAR (Figure 6, G–I). Similarly, fibroblasts transfected with WT uPAR cDNA did not differ from nontransfected (data not shown). Finally, transfection with GFP alone also did not inhibit myofibroblast transformation (Figure 6, J–L). These data suggest that retention of full-length uPAR inhibited TGFβ-stimulated myofibroblast differentiation.

Full-Length uPAR in Liver and Lung Cells

To determine whether fibroblasts and myofibroblasts from other tissues behaved similarly to corneal fibroblasts and myofibroblasts, human hepatic stellate cells and normal human lung fibroblasts were grown for 72 h in either FGF or TGFβ, and they were immunostained for α-SMA (Figure 7A). Similar to corneal cells, after addition of TGFβ, both liver and lung cells differentiate into myofibroblasts that organize α-SMA actin stress fibers, whereas in the presence of FGF-2, they maintain fibroblast morphology. To investi-

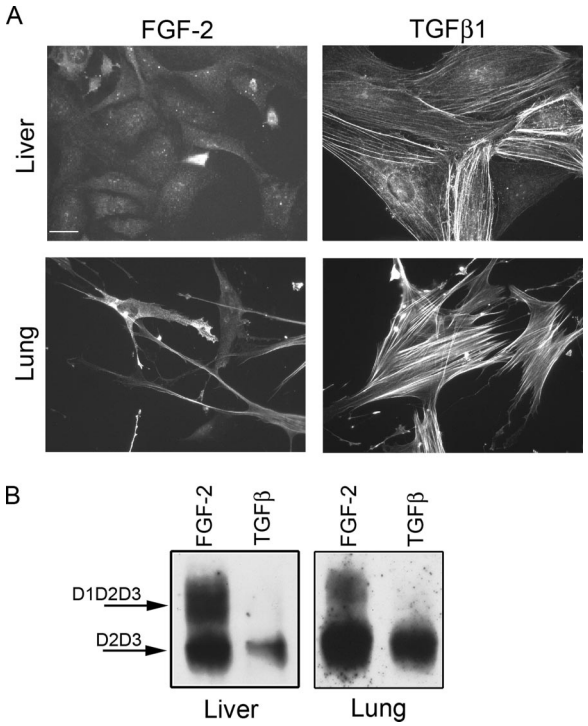

Figure 7. FGF-2 protects uPAR from cleavage in liver and lung fibroblasts. TGFβ-treated cells became myofibroblasts and expressed cleaved uPAR (D2D3). Human hepatic stellate cells (liver, LX2) and normal human lung fibroblasts (LL24) were seeded in SSFM-FGF or SSFM-TGFβ, and cells were grown for 72 h. (A) Cells were immunostained with antibody to α-SMA. Bar, 20 μm. (B) Cell lysates were probed by Western blot for total uPAR. The images shown are representative of two experiments.

gate the relationship of cell phenotype to uPAR expression and cleavage, a Western blot for total uPAR by using the D2 antibody was performed on lysates of liver and lung cells grown with either FGF or TGFβ for 72 h (Figure 7B). The increased expression of full-length uPAR in FGF-2–treated fibroblasts demonstrated that retention of full-length uPAR in FGF-2–treated cells is a general mechanism and not specific to the cornea.

DISCUSSION

We have focused on the potential contributions of uPA/uPAR to wound healing and specifically on the role of uPA and uPAR in the conversion of fibroblasts to myofibroblasts. In this report, we demonstrated that uPA and uPAR were expressed de novo in activated fibroblasts but that they were down-regulated in myofibroblasts. Specifically, uPA activity was stimulated by FGF-2, and it was significantly decreased by TGFβ1. Furthermore, although we detected cleaved uPAR in fibroblasts as well as myofibroblasts, only FGF-2–treated cells continued to express full-length uPAR, which suggests that FGF-2 promotes the resynthesis of full-length uPAR and that TGFβ does not. Thus, over a 7-d period of TGFβ treatment, the proportion of full-length-to-cleaved uPAR steadily decreased, and eventually the receptor expression was almost completely absent. Finally, retention of full-length uPAR was shown to prevent the fibroblast to myofibroblast transition as overexpression of a cDNA for a noncleavable form of uPAR prevented myofibroblast differentiation in the presence of TGFβ1.

After wounding in vivo, growth factors such as FGF-2 and TGFβ1, and new matrix molecules such as vitronectin and fibronectin, are secreted into the collagenous matrix (Maguen *et al*., 2002). Depending on spatial and temporal interactions within their environment, the balance of these and other growth factors and their interactions with matrix determine the cellular repair program. Our data suggest that during the migration phase, FGF-2 exerts a dominant effect over TGFβ, resulting in the retention of full-length uPAR and the maintenance of the fibroblast phenotype. In the presence of full-length uPAR, the binding of uPAR to uPA, vitronectin, and integrins results in a promigratory phase (Wei *et al*., 1996; Waltz *et al*., 1997; Montuori *et al*., 2002; Czekay *et al*., 2003). When uPAR is cleaved, it no longer interacts with uPA, vitronectin, or integrins. Thus, the extracellular uPA protease pathway and the intracellular uPA-stimulated signaling are halted. In addition, cleaved uPAR may promote greater cell adhesion by impeding cell detachment, because PAI-1 binding to uPA on full-length uPAR promotes cell detachment through the endocytosis of the uPA/uPAR/integrin/LRP complex (Nykjaer *et al*., 1997; Czekay *et al*., 2003). Furthermore, cleaved uPAR no longer interacts with integrins, resulting in altered integrin function that promotes an increase in cell adhesion on collagen, fibronectin, and laminin (Montuori *et al*., 2002). These data suggest that in the absence of the integrin/uPAR interaction, the adhesive functions of integrins in focal adhesions become dominant. Our model predicts that early after wounding, when both FGF-2 and TGFβ are elevated, FGF-2 would stimulate uPA signaling through the retention of full-length uPAR on the cell surface, whereas TGFβ-stimulated PAI-1 secretion would promote cell detachment and migration. In the absence of the FGF-2 stimulus, full-length uPAR expression would steadily decrease leaving cleaved uPAR on the cell surface before total inhibition of uPAR synthesis. In the later stages of wound healing, decreased uPA activity, decreased cycling of uPA/uPAR/integrin/LRP-induced detachment, and lack of integrin/uPAR interaction would result in increased cell adhesion. The resultant stabilized focal adhesions would provide the tension between the matrix and the cell surface required for the assembly of α-SMA stress fibers that are characteristic of the myofibroblast (Hinz and Gabbiani, 2003).

Signal transduction studies involving uPAR have focused on signaling initiated by uPA binding to full-length uPAR and transmitted through a uPAR transmembrane binding partner to induce migration and proliferation. uPAR is known to partner with integrins, $\alpha5\beta1$ and $\alpha v\beta3$, as well as EGFR with the resultant activation of the mitogen-activated protein (MAP) kinase pathway (Aguirre Ghiso *et al*., 1999; Degryse *et al*., 2001; Liu *et al*., 2002). uPAR also binds to GP130, activating the Janus tyrosine kinase 1/signal transducer and activator of transcription 1 pathway (Koshelnick *et al*., 1997; Dumler *et al*., 1998, 1999) and platelet-derived growth factor receptor, activating the Tyk2/phosphatidylinositol 3-kinase pathway (Kiian *et al*., 2003; Kiyan *et al*., 2005). Although uPAR also binds to the G protein-coupled chemokine *N*-formyl-L-methionyl-L-leucyl-L-phenylalanine receptor (Gyetko *et al*., 1994), its mechanism of action is unusual in that uPA and the D1 domain of uPAR are not required to induce chemotaxis (Montuori *et al*., 2002). To directly compare the downstream signals from full-length and cleaved uPAR, Mazzieri *et al*. (2006) overexpressed WT-uPAR (cleavable) and noncleavable uPAR cDNA in L-cells, which lack endogenous uPA/uPAR expression. The WT-uPAR cDNA promoted MAP kinase signaling, whereas the noncleavable uPAR construct did not (Mazzieri *et al*., 2006). These data together with our finding that uPAR was cleaved in both FGF-2– and TGFβ1-treated cells suggests that al-

though uPAR cleavage down-regulates uPAR function, it also promotes intracellular signaling that is key to cellular function. Furthermore, the finding that overexpression of noncleavable uPAR prevented myofibroblast differentiation suggests that signaling through the MAP kinase pathway may be required to promote the fibroblast to myofibroblast transition. The importance of uPAR cleavage to signaling cascades and cell programs needs further investigation.

Toward the goal of identifying the protease(s) that cleaves uPAR in the linker region between D1 and D2, protease inhibitors were tested for their ability to prevent uPAR cleavage. Although proteases such as plasmin, uPA, and trypsin are known to cleave uPAR in the linker region between D1 and D2 (Montuori *et al*., 2005), the inability of leupeptin to inhibit uPAR cleavage suggests they are not involved here (Zimmerman *et al*., 1978). Similarly, metalloproteases cleave uPAR in the linker region, but uPAR cleavage was not inhibited by the general metalloprotease inhibitor GM6001. However, GM6001 does not inhibit all matrix metalloproteinases, thus, the possibility that an matrix metalloproteinase is cleaving uPAR must still be considered. We found that the serine protease inhibitor AEBSF and the chymotrypsin inhibitor chymostatin prevented uPAR cleavage and subsequently prevented TGFβ1-stimulated myofibroblast differentiation. From the inhibitor data, we propose cathepsin G and chymotrypsin as candidates for the proteases that cleave uPAR, because both would be inhibited by AEBSF and chymostatin. Furthermore, both cleave uPAR in the D1D2 linker region at tyrosine 87 (Ploug *et al*., 1994, Beaufort *et al*., 2004) corresponding to a mutated site in the noncleavable uPAR construct. Expression of this noncleavable construct also prevented myofibroblast differentiation. These data suggest that Y87 is a target for controlling myofibroblast differentiation. Our finding that the general serine protease inhibitor aprotinin did not prevent uPAR cleavage but that AEBSF did is consistent with the possibility that a membrane-bound cathepsin G is cleaving uPAR. This hypothesis is supported by the fact that small inhibitors in the range of 8–10 kDa, such as aprotinin, do not effectively inhibit cathepsin G in its membrane-bound form. In contrast, aprotinin does inhibit secreted chymotrypsin and secreted cathepsin G (Owen and Campbell, 1998). Finding cathepsin G in both FGF-2–treated and TGFβ-treated cells is consistent with cleavage of uPAR in both fibroblasts and myofibroblasts. Identifying the protease that cleaves uPAR is this system will be important for modulating the ratio of full-length-to-cleaved uPAR on the cell surface and, therefore, potentially controlling myofibroblast differentiation.

In regenerative healing, the repaired tissue is not fibrotic, and it regains its original strength. Migration of fibroblasts into the wound provides a cellular source of new matrix, to repair the wound. At the wound margin, fibroblasts differentiate into myofibroblasts, which promote wound closure, but few if any myofibroblasts remain in a healed wound. However, wound-healing pathways can malfunction, resulting in either incomplete repair or excessive repair (fibrosis). In incompletely healed wounds, fibroblasts do not migrate into the wound; thus, the strength of the tissue is not regained. In fibrotically healed wounds, fibroblasts migrate into the wound and differentiate into myofibroblasts, but these myofibroblasts are more abundant than normal, and they persist in the healed wound, resulting in scar tissue. Similarly, liver cirrhosis and idiopathic lung fibrosis are characterized by an abundance of myofibroblasts. Our data demonstrate that the patterns of uPAR expression and cleavage are similar for cornea, liver, and lung, suggesting that uPAR-mediated myofibroblast regulation is not unique to the cornea. Because an abundance of myofibroblasts and fibrotic scarring is correlated with excessive levels of TGFβ1, several wound healing studies have investigated the potential of inhibiting TGFβ1 with reagents such as anti-TGFβ1 antibodies to reduce fibrosis (Shah *et al*., 1992; Jester *et al*., 1997; Thom *et al*., 1997; Moller-Pedersen *et al*., 1998). Although fibrosis is inhibited with anti-TGFβ1 antibodies, cell migration and proliferation are also inhibited (Carrington *et al*., 2006). Thus, the determination of more specific targets that promote fibroblast migration and mediate the conversion of fibroblasts to myofibroblasts, such as the uPA pathway, warrant investigation.

ACKNOWLEDGMENTS

We are grateful to Dr. Lilliana Ossowski for generous contribution of reagents and for insightful comments about the manuscript, to Dr. Robert Hennigan for microscopy expertise, and to Leah Kang for technical assistance. This research was supported by National Institutes of Health (NIH) grants F32 EY07049 and R01 EYO17030 (to A.M.B.), R01 EY09414 (to S.K.M.), R01 EY14168 (to S.S.T.), and National Eye Institute core grant P30-EY001867 and a Research to Prevent Blindness grant. Microscopy was performed at the MSSM-Microscopy Shared Research Facility, supported, in part, with funding from NIH-National Cancer Institute shared resources grant 1 R24 CA095823 and National Science Foundation Major Research Instrumentation grant DBI-9724504.

REFERENCES

Abe, M., Harpel, J. G., Metz, C. N., Nunes, I., Loskutoff, D. J., and Rifkin, D. B. (1994). An assay for transforming growth factor-beta using cells transfected with a plasminogen activator inhibitor-1 promoter-luciferase construct. Anal. Biochem. *216*, 276–284.

Aguirre Ghiso, J., Kovalski, K., and Ossowski, L. (1999). Tumor dormancy induced by downregulation of urokinase receptor in human carcinoma involves integrin and MAPK signaling. J. Cell Biol. *147*, 89–104.

Baker, M. S., Liang, X. M., and Doe, W. F. (1992). Occupancy of the cancer cell urokinase receptor (uPAR): effects of acid elution and exogenous uPA on cell surface urokinase (uPA). Biochim. Biophys. Acta *1117*, 143–152.

Beaufort, N., Leduc, D., Rousselle, J. C., Magdolen, V., Luther, T., Namane, A., Chignard, M., and Pidard, D. (2004). Proteolytic regulation of the urokinase receptor/CD87 on monocytic cells by neutrophil elastase and cathepsin G. J. Immunol. *172*, 540–549.

Behrendt, N., Ploug, M., Patthy, L., Houen, G., Blasi, F., and Dano, K. (1991). The ligand-binding domain of the cell surface receptor for urokinase-type plasminogen activator. J. Biol. Chem. *266*, 7842–7847.

Bernstein, A. M., Greenberg, R. S., Taliana, L., and Masur, S. K. (2004). Urokinase anchors uPAR to the actin cytoskeleton. Invest. Ophthalmol. Vis. Sci. *45*, 2967–2977.

Blasi, F., and Carmeliet, P. (2002). uPAR: a versatile signalling orchestrator. Nat. Rev. Mol. Cell Biol. *3*, 932–943.

Carrington, L. M., Albon, J., Anderson, I., Kamma, C., and Boulton, M. (2006). Differential regulation of key stages in early corneal wound healing by TGF-beta isoforms and their inhibitors. Invest. Ophthalmol. Vis. Sci. *47*, 1886–1894.

Czekay, R. P., Aertgeerts, K., Curriden, S. A., and Loskutoff, D. J. (2003). Plasminogen activator inhibitor-1 detaches cells from extracellular matrices by inactivating integrins. J. Cell Biol. *160*, 781–791.

Czekay, R. P., Kuemmel, T. A., Orlando, R. A., and Farquhar, M. G. (2001). Direct binding of occupied urokinase receptor (uPAR) to LDL receptor-related protein is required for endocytosis of uPAR and regulation of cell surface urokinase activity. Mol. Biol. Cell *12*, 1467–1479.

Degryse, B., Orlando, S., Resnati, M., Rabbani, S. A., and Blasi, F. (2001). Urokinase/urokinase receptor and vitronectin/alpha(v) beta(3) integrin induce chemotaxis and cytoskeleton reorganization through different signaling pathways. Oncogene *20*, 2032–2043.

Desmouliere, A., Darby, I. A., and Gabbiani, G. (2003). Normal and pathologic soft tissue remodeling: role of the myofibroblast, with special emphasis on liver and kidney fibrosis. Lab. Invest. *83*, 1689–1707.

Desmouliere, A., Redard, M., Darby, I., and Gabbiani, G. (1995). Apoptosis mediates the decrease in cellularity during the transition between granulation tissue and scar. Am. J. Pathol. *146*, 56–66.

Dumler, I., Kopmann, A., Weis, A., Mayboroda, O., Wagner, K., Gulba, D., and Haller, H. (1999). Urokinase activates the Jak/Stat signal transduction pathway in human vascular endothelial cells. Arterioscler. Thromb. Vasc. Biol. *19*, 290–297.

Dumler, I., Weis, A., Mayboroda, O., Maasch, C., Jerke, U., Haller, H., and Gulba, D. (1998). The Jak/Stat pathway and urokinase receptor signaling in human aortic vascular smooth muscle cells. J. Biol. Chem. *273*, 315–321.

Gabbiani, G. (2003). The myofibroblast in wound healing and fibrocontractive diseases. J. Pathol. *200*, 500–503.

Garwicz, D., Lindmark, A., and Gullberg, U. (1995). Human cathepsin G lacking functional glycosylation site is proteolytically processed and targeted for storage in granules after transfection to the rat basophilic/mast cell line RBL or the murine myeloid cell line 32D. J. Biol. Chem. *270*, 28413–28418.

Gyetko, M. R., Todd, R. F., 3rd, Wilkinson, C. C., and Sitrin, R. G. (1994). The urokinase receptor is required for human monocyte chemotaxis in vitro. J. Clin. Invest. *93*, 1380–1387.

Hinz, B., and Gabbiani, G. (2003). Mechanisms of force generation and transmission by myofibroblasts. Curr. Opin. Biotechnol. *14*, 538–546.

Hoyer-Hansen, G., Behrendt, N., Ploug, M., Dano, K., and Preissner, K. T. (1997). The intact urokinase receptor is required for efficient vitronectin binding: receptor cleavage prevents ligand interaction. FEBS Lett. *420*, 79–85.

Hoyer-Hansen, G., Ronne, E., Solberg, H., Behrendt, N., Ploug, M., Lund, L. R., Ellis, V., and Dano, K. (1992). Urokinase plasminogen activator cleaves its cell surface receptor releasing the ligand-binding domain. J. Biol. Chem. *267*, 18224–18229.

Jester, J. V., Barry-Lane, P. A., Petroll, W. M., Olsen, D. R., and Cavanagh, H. D. (1997). Inhibition of corneal fibrosis by topical application of blocking antibodies to TGF beta in the rabbit. Cornea *16*, 177–187.

Jester, J. V., Huang, J., Barry-Lane, P. A., Kao, W. W., Petroll, W. M., and Cavanagh, H. D. (1999). Transforming growth factor(beta)-mediated corneal myofibroblast differentiation requires actin and fibronectin assembly. Invest. Ophthalmol. Vis. Sci. *40*, 1959–1967.

Jester, J. V., Petroll, W. M., Barry, P. A., and Cavanagh, H. D. (1995). Expression of alpha-smooth muscle (alpha-SM) actin during corneal stromal wound healing. Invest. Ophthalmol. Vis. Sci. *36*, 809–819.

Kanemaru, K., Meckelein, B., Marshall, D. C., Sipe, J. D., and Abraham, C. R. (1996). Synthesis and secretion of active alpha 1-antichymotrypsin by murine primary astrocytes. Neurobiol. Aging *17*, 767–771.

Kiian, I., Tkachuk, N., Haller, H., and Dumler, I. (2003). Urokinase-induced migration of human vascular smooth muscle cells requires coupling of the small GTPases RhoA and Rac1 to the Tyk2/PI3-K signalling pathway. Thromb. Haemost. *89*, 904–914.

Kiyan, J., Kiyan, R., Haller, H., and Dumler, I. (2005). Urokinase-induced signaling in human vascular smooth muscle cells is mediated by PDGFR-beta. EMBO J. *24*, 1787–1797.

Koshelnick, Y., Ehart, M., Hufnagl, P., Heinrich, P. C., and Binder, B. R. (1997). Urokinase receptor is associated with the components of the JAK1/STAT1 signaling pathway and leads to activation of this pathway upon receptor clustering in the human kidney epithelial tumor cell line TCL-598. J. Biol. Chem. *272*, 28563–28567.

Liu, D., Aguirre Ghiso, J., Estrada, Y., and Ossowski, L. (2002). EGFR is a transducer of the urokinase receptor initiated signal that is required for in vivo growth of a human carcinoma. Cancer Cell *1*, 445–457.

Maguen, E., Zorapapel, N. C., Zieske, J. D., Ninomiya, Y., Sado, Y., Kenney, M. C., and Ljubimov, A. V. (2002). Extracellular matrix and matrix metalloproteinase changes in human corneas after complicated laser-assisted in situ keratomileusis (LASIK). Cornea *21*, 95–100.

Maltseva, O., Petridou, S., and Masur, S. K. (1998). Cytokine regulation of corneal fibroblast and myofibroblast phenotypes. Invest. Ophthalmol. Vis. Sci. *39*, S775.

Masur, S. K., Cheung, J. K., and Antohi, S. (1993). Identification of integrins in cultured corneal fibroblasts and in isolated keratocytes. Invest. Ophthalmol. Vis. Sci. *34*, 2690–2698.

Mazzieri, R., D'Alessio, S., Kenmoe, R. K., Ossowski, L., and Blasi, F. (2006). An uncleavable uPAR mutant allows dissection of signaling pathways in uPA-dependent cell migration. Mol. Biol. Cell *17*, 367–378.

Mohan, R. R., Hutcheon, A. E., Choi, R., Hong, J., Lee, J., Ambrosio, R., Jr., Zieske, J. D., and Wilson, S. E. (2003). Apoptosis, necrosis, proliferation, and myofibroblast generation in the stroma following LASIK and PRK. Exp. Eye Res. *76*, 71–87.

Moller-Pedersen, T., Cavanagh, H. D., Petroll, W. M., and Jester, J. V. (1998). Neutralizing antibody to TGFbeta modulates stromal fibrosis but not regression of photoablative effect following PRK. Curr. Eye Res. *17*, 736–747.

Montuori, N., Carriero, M. V., Salzano, S., Rossi, G., and Ragno, P. (2002). The cleavage of the urokinase receptor regulates its multiple functions. J. Biol. Chem. *277*, 46932–46939.

Montuori, N., Rossi, G., and Ragno, P. (1999). Cleavage of urokinase receptor regulates its interaction with integrins in thyroid cells. FEBS Lett. *460*, 32–36.

Montuori, N., Visconte, V., Rossi, G., and Ragno, P. (2005). Soluble and cleaved forms of the urokinase-receptor: degradation products or active molecules? Thromb. Haemost. *93*, 192–198.

Nakayasu, K. (1988). Stromal changes following removal of epithelium in rat cornea. Jpn. J. Ophthalmol. *32*, 113–125.

Netto, M. V., Mohan, R. R., Ambrosio, R., Jr., Hutcheon, A. E., Zieske, J. D., and Wilson, S. E. (2005). Wound healing in the cornea: a review of refractive surgery complications and new prospects for therapy. Cornea *24*, 509–522.

Nykjaer, A., Conese, M., Christensen, E. I., Olson, D., Cremona, O., Gliemann, J., and Blasi, F. (1997). Recycling of the urokinase receptor upon internalization of the uPA:serpin complexes. EMBO J. *16*, 2610–2620.

Owen, C. A., and Campbell, E. J. (1998). Angiotensin II generation at the cell surface of activated neutrophils: novel cathepsin G-mediated catalytic activity that is resistant to inhibition. J. Immunol. *160*, 1436–1443.

Ploug, M., Ellis, V., and Dano, K. (1994). Ligand interaction between urokinase-type plasminogen activator and its receptor probed with 8-anilino-1-naphthalenesulfonate. Evidence for a hydrophobic binding site exposed only on the intact receptor. Biochemistry *33*, 8991–8997.

Ragno, P. (2006). The urokinase receptor: a ligand or a receptor? Story of a sociable molecule. Cell Mol. Life Sci. *63*, 1028–1037.

Shah, M., Foreman, D. M., and Ferguson, M. W. (1992). Control of scarring in adult wounds by neutralising antibody to transforming growth factor beta. Lancet *339*, 213–214.

Stefansson, S., and Lawrence, D. A. (2003). Old dogs and new tricks: proteases, inhibitors, and cell migration. Sci. STKE *2003*, pe24.

Stoppelli, M. P., Tacchetti, C., Cubellis, M. V., Corti, A., Hearing, V. J., Cassani, G., Appella, E., and Blasi, F. (1986). Autocrine saturation of pro-urokinase receptors on human A431 cells. Cell *45*, 675–684.

Thom, S. B., Myers, J. S., Rapuano, C. J., Eagle, R. C., Jr., Siepser, S. B., and Gomes, J. A. (1997). Effect of topical anti-transforming growth factor-beta on corneal stromal haze after photorefractive keratectomy in rabbits. J. Cataract Refract. Surg. *23*, 1324–1330.

Tomasek, J. J., Gabbiani, G., Hinz, B., Chaponnier, C., and Brown, R. A. (2002). Myofibroblasts and mechano-regulation of connective tissue remodelling. Nat. Rev. Mol. Cell Biol. *3*, 349–363.

Tripathi, R. C., Tripathi, B. J., and Park, J. K. (1990). Localization of urokinase-type plasminogen activator in human eyes: an immunocytochemical study. Exp. Eye. Res. *51*, 545–552.

Twining, S. S., Fukuchi, T., Yue, B. Y., Wilson, P. M., and Zhou, X. (1994). Alpha 1-antichymotrypsin is present in and synthesized by the cornea. Curr. Eye Res. *13*, 433–439.

Twining, S. S., Zhou, X., Schulte, D. P., Wilson, P. M., Fish, B., and Moulder, J. (1996). Effect of vitamin A deficiency on the early response to experimental *Pseudomonas* keratitis. Invest. Ophthalmol. Vis. Sci. *37*, 511–522.

Waltz, D. A., Natkin, L. R., Fujita, R. M., Wei, Y., and Chapman, H. A. (1997). Plasmin and plasminogen activator inhibitor type 1 promote cellular motility by regulating the interaction between the urokinase receptor and vitronectin. J. Clin. Invest. *100*, 58–67.

Warejcka, D. J., Vaughan, K. A., Bernstein, A. M., and Twining, S. S. (2005). Differential conversion of plasminogen to angiostatin by human corneal cell populations. Mol. Vis. *11*, 859–868.

Webb, D. J., Nguyen, D. H., Sankovic, M., and Gonias, S. L. (1999). The very low density lipoprotein receptor regulates urokinase receptor catabolism and breast cancer cell motility in vitro. J. Biol. Chem. *274*, 7412–7420.

Wei, Y., Lukashev, M., Simon, D. I., Bodary, S. C., Rosenberg, S., Doyle, M. V., and Chapman, H. A. (1996). Regulation of integrin function by the urokinase receptor. Science *273*, 1551–1555.

Weimar, V. (1957). The transformation of corneal stromal cells to fibroblasts in corneal wound healing. Am. J. Opthalmol. *44*, 173–182.

Whitelock, R. B., Fukuchi, T., Zhou, L., Twining, S. S., Sugar, J., Feder, R. S., and Yue, B. Y. (1997). Cathepsin G, acid phosphatase, and alpha 1-proteinase inhibitor messenger RNA levels in keratoconus corneas. Invest. Ophthalmol. Vis. Sci. *38*, 529–534.

Zimmerman, M., Quigley, J. P., Ashe, B., Dorn, C., Goldfarb, R., and Troll, W. (1978). Direct fluorescent assay of urokinase and plasminogen activators of normal and malignant cells: kinetics and inhibitor profiles. Proc. Natl. Acad. Sci. USA *75*, 750–753.